DEEP 10 AND 18 MICRON IMAGING OF THE HR 4796A CIRCUMSTELLAR DISK: TRANSIENT DUST PARTICLES AND TENTATIVE EVIDENCE FOR A BRIGHTNESS ASYMMETRY[1]

C. M. TELESCO,[2] R. S. FISHER,[2] R. K. PIÑA,[2] R. F. KNACKE,[3] S. F. DERMOTT,[2] M. C. WYATT,[2] K. GROGAN,[2] E. K. HOLMES,[2] A. M. GHEZ,[4] L. PRATO,[4] L. W. HARTMANN,[5] AND R. JAYAWARDHANA[5]

ABSTRACT

We present new 10.8 and 18.2 μm images of HR 4796A, a young A0 V star that was recently discovered to have a spectacular, nearly edge-on, circumstellar disk prominent at ~ 20 μm (Jayawardhana and coworkers; Koerner and coworkers). These new images, obtained with OSCIR (the University of Florida Observatory Spectrometer/Camera for the Infrared) at Keck II, show that the disk's size at 10 μm is comparable to its size at 18 μm. Therefore, the 18 μm–emitting dust may also emit some, or all, of the 10 μm radiation. Using these multiwavelength images, we determine a "characteristic" diameter of 2–3 μm for the mid-infrared–emitting dust particles if they are spherical and composed of astronomical silicates. Particles this small are expected to be blown out of the system by radiation pressure in a few hundred years, and therefore these particles are unlikely to be primordial. Rather, as inferred in a companion paper (Wyatt and coworkers), they are probably products of collisions that dominate both the creation and the destruction of dust in the HR 4796A disk. Dynamical modeling of the disk, the details of which are presented in the companion paper, indicates that the disk surface density is relatively sharply peaked near 70 AU, which agrees with the mean annular radius deduced by Schneider and coworkers from their NICMOS images. Interior to 70 AU, the model density drops steeply by a factor of 2 between 70 and 60 AU, falling to zero by 45 AU, which corresponds to the edge of the previously discovered central hole; in the context of the dynamical models, this "soft" edge for the central hole occurs because the dust particle orbits are noncircular. The optical depth of mid-infrared–emitting dust in the hole is $\sim 3\%$ of the optical depth in the disk, and the hole is therefore relatively very empty. We present evidence ($\sim 1.8\sigma$ significance) for a brightness asymmetry that may result from the presence of the hole and the gravitational perturbation of the disk particle orbits by the low-mass stellar companion or a planet. This "pericenter glow," which must still be confirmed, results from a very small (a few AU) shift of the disk's center of symmetry relative to the central star HR 7496A; one side of the inner boundary of the annulus is shifted toward HR 4796A, thereby becoming warmer and more infrared-emitting. The possible detection of pericenter glow implies that the detection of even complex dynamical effects of planets on disks is within reach.

Subject headings: circumstellar matter — infrared: stars — stars: individual (HR 4796A)

1. INTRODUCTION

Planets form in dusty circumstellar disks, and so the exploration of circumstellar disks contributes fundamentally to a broader understanding of the origin and evolution of our own and other planetary systems. Vega-type disks, often called debris disks, are those that surround main-sequence stars (see the review by Backman & Paresce 1993). Unlike the disks surrounding pre–main-sequence stars, the dust masses of debris disks are generally much smaller than 0.01 $M_\odot$, which is roughly the minimum mass required for the formation of a planetary system like our own (see, e.g., Beckwith & Sargent 1993; Strom et al. 1993). The lower mass of debris disks conforms with the expectation that

disks disperse with time as the material accretes onto the stars, forms planets, and/or is blown out of the systems (e.g., Strom et al. 1993). The elucidation of these evolutionary processes is a key challenge of observational astronomy.

High angular resolution, multiwavelength imaging of circumstellar disks can provide unique insight into these processes, since a disk's detailed structure should bear traces of its history and of any developing or mature planets. Until recently, the disk surrounding the A5 star β Pictoris (Smith & Terrile 1984; Telesco et al. 1988; Lagage & Pantin 1994; Kalas & Jewitt 1995) was the only debris disk that was spatially well resolved at optical or infrared wavelengths. However, many new results have emerged over the past few years, including the following: possible optical imaging of a disk around the binary star BD $+ 31°643$ (Kalas & Jewitt 1997); submillimeter imaging of impressive structure in several debris disks, including the class archetype Vega (Holland et al. 1998; Greaves et al. 1998); and ~ 20 μm imaging of the nearly edge-on-disk around the A0 V star HR 4796 (Jayawardhana et al. 1998, hereafter J98; Koerner et al. 1998, hereafter K98), results that were recently complemented with NICMOS images revealing what appears to be a sharply defined ring (Schneider et al. 1999).

Here we present new 10.8 and 18.2 μm images, obtained at the Keck II telescope, of the HR 4796A debris disk. Jura (1991) first drew attention to HR 4796, pointing out that its

[2] Department of Astronomy, University of Florida, Gainesville, FL 32611; telesco@astro.ufl.edu, fisher@astro.ufl.edu, rpina@astro.ufl.edu, dermott@astro.ufl.edu, grogan@astro.ufl.edu, holmes@astro.ufl.edu, wyatt@astro.ufl.edu.

[3] School of Science, Pennsylvania State University at Erie, Station Road, Erie, PA 16563; rfk2@psu.edu.

[4] Department of Astronomy, University of California, Los Angeles, CA 90095; ghez@athena.astro.ucla.edu, 1prato@minerva.astro.ucla.edu.

[5] Harvard-Smithsonian Center for Astrophysics, 60 Garden Street, Cambridge, MA 02138; hartmann@fuor.harvard.edu, rayjay@shakti.harvard.edu.

Filters	N	1HW 18
λ_0 (μm)	10.8	18.2
$\Delta\lambda$ (μm)..................	5.3	1.7
Integration time (s)[a]......	2784	3480
Total F_ν (Jy)[b]	0.188 ± 0.047	0.905 ± 0.130
1σ noise/pixel (mJy)......	0.014	0.15
Stellar F_ν (Jy)[c]	0.150	0.048
α Sco F_ν (Jy)..............	...	817
γ Aql F_ν (Jy)..............	...	26
δ Vir F_ν (Jy)..............	142	...

[a] Integration times correspond to both halves of the chopper cycle. They are the sum of the times for which the source itself and the reference sky position were projected onto the detector.

[b] The uncertainties for the 10.8 and 18.2 μm flux densities, which are based on the reproducibility of standard-star fluxes, are principally due to the presence of light cirrus clouds. This problem was more severe for the 10.8 μm than for the 18.2 μm image.

[c] The 10.8 μm photospheric flux density was derived by Jura et al. (1998) by extrapolating the K-band (2.2 μm) flux density to 10.8 μm using the Kurucz (1979) model atmosphere for $T = 9500$ K and $\log g = 4.0$. The 18.2 μm flux density is derived assuming the 10.8–18.2 μm flux ratio of Vega.

infrared spectral energy distribution resembles that of β Pic but with twice the IR excess ($L_{\rm IR}/L_*$). The *IRAS* data showed no discernible emission from dust hotter than ~ 110 K, implying that there is little dust closer to the star than 40 AU (Jura et al. 1993). The existence of one or more planets was suggested as one of the possible causes of this central hole in the dust distribution (Jura et al. 1995, 1998). J98 and K98 determined that the disk's diameter is $\sim 3''$, which corresponds to 200 AU at the star's distance of 67 pc, and they confirmed directly the existence of the central hole. An especially significant aspect of the discovery is that, based on isochrone fitting and the strong lithium absorption line, the presumably coeval companion HR 4796B, located $7''.7$ away at P.A. $= 226°$ (Jura et al. 1993), is an M2–M3 pre–main-sequence star with an age tightly constrained to be $(8 \pm 3) \times 10^6$ yr (Stauffer et al. 1995; Jura et al. 1998). Observational and theoretical studies of our solar system, including chronological data for meteorites, suggest that $\sim 10^7$ yr is a reasonable estimate of the timescale for the duration of the solar nebula and the growth of the planets to nearly their final masses (see reviews by Lissauer 1993 and Podosek & Cassen 1994). Thus, the constraints on the age of HR 4796A place it within a critical stage of planetary disk evolution.

Our new images clarify the structure of the central clearing zone, or hole, which may be indirect evidence for a planet orbiting HR 4796A (see, e.g., Roques et al. 1994). They may also reveal an asymmetry in the disk, possibly confirmed by the NICMOS images (Schneider et al. 1999), which could reflect the influence of the stellar companion or a hypothetical planet. Finally, these multiwavelength data provide a reasonable basis for estimating a characteristic size for the mid-infrared–emitting dust particles, an estimate with implications for our understanding of the disk evolution. Our results and discussion complement those in a companion paper by Wyatt et al. (1999, hereafter W99).

2. MID-INFRARED IMAGING WITH OSCIR AT KECK II

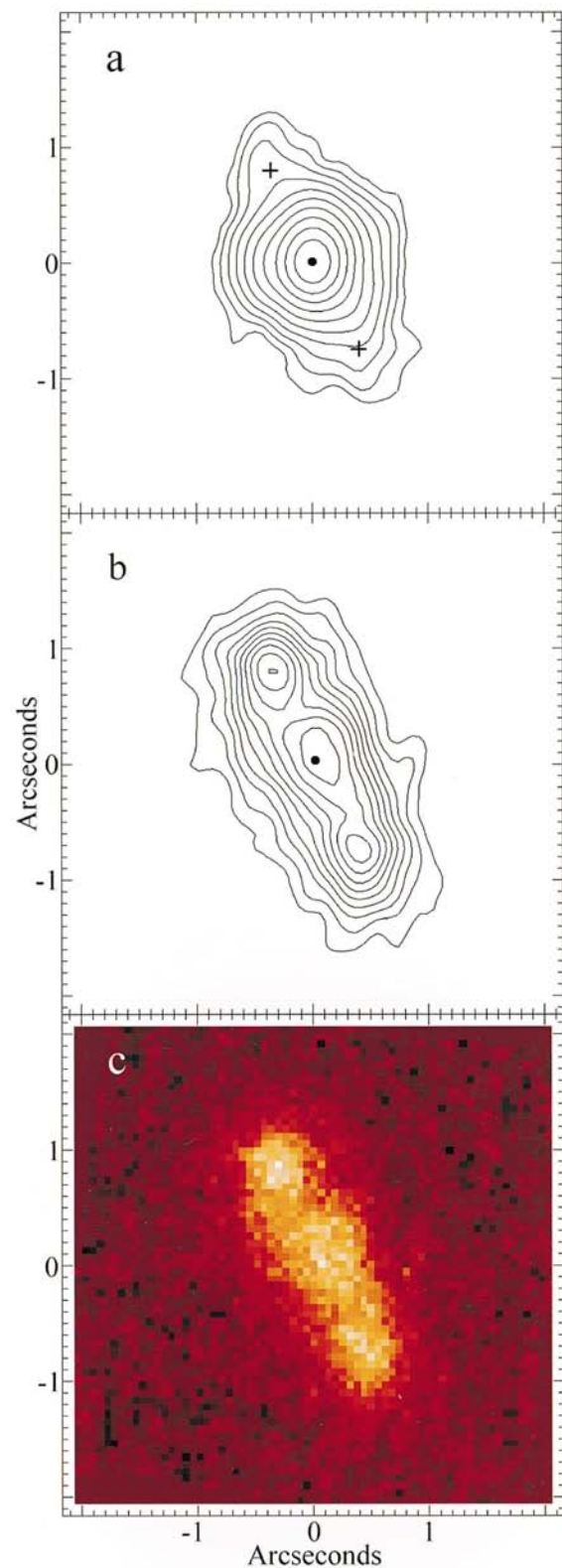We imaged HR 4796A in the N (10.8 μm) and IHW 18

FIG. 1.—Images of HR 4796A made with OSCIR. North is up, and east is to the left. The images from which the two contour plots were constructed were smoothed with a 3 pixel (FWHM), or $0''.19$, Gaussian. For both contour plots, the lowest contour level is about 4 times the smoothed noise. (*a*) 10.8 μm image with contours (mJy arcsec^{-2}) spaced logarithmically at 6.4, 9.9, 15, 23, 36, 55, 85, 132, 203, and 312. The filled circle is the location of the peak brightness, with the value 480 mJy arcsec^{-2}. The crosses indicate the positions of the 18.2 μm lobes. (*b*) 18.2 μm image with contours (mJy arcsec^{-2}) spaced linearly at 58, 93, 128, 163, 198, 234, 269, 304, 339, and 374. The filled circle indicates the presumed position of the star, where the brightness is 362 mJy arcsec^{-2}; (*c*) Unsmoothed version, with linear brightness levels, of the 18.2 μm image.

(18.2 μm) bands at the Keck II Telescope in 1998 May 7–12 with OSCIR, the University of Florida mid-infrared imager/spectrometer. OSCIR contains a 128 × 128 pixel, Si:As Blocked Impurity Band (BIB) array developed by Boeing. The plate scale was 0″.062 pixel⁻¹ with the f/40 chopping secondary at the Keck II visitor bent-Cassegrain port, which gave an array field of view of 7″.9 × 7″.9. We used a guide star and the off-axis autoguider, which ensured excellent tracking and image stability, and the standard chop/nod technique, with a chop frequency of 4 Hz and a throw of 8″ in declination. The stars α Sco, γ Aql, and δ Vir were used for flux calibration. The seeing was generally very good for our observations. Typical values of the FWHM intensity of the observed point-spread functions (PSFs) were 0″.32 at 10.8 μm and 0″.45 at 18.2 μm, compared to the diffraction-limited values (λ/D) of 0″.22 and 0″.37, respectively. Quadratic subtraction of these implies 10–20 μm "seeing" of ~0″.2–0″.3 (which may include other contributions, e.g., from autoguider jitter). The diffraction limits at 10 and 18 μm correspond to 4 and 6 pixels, respectively, and thus OSCIR spatially samples the diffraction-limited PSF more finely than conventional Nyquist sampling. We encountered light cirrus throughout much of our Keck run. By comparing observations within and among the nights, we believe that we have been able generally to remove the data for which the photometry is most uncertain. However, because of the cirrus, some unquantifiable uncertainty remains in the photometry. Key properties of the obser-vations, including flux densities and noise estimates, are listed in Table 1. The images are presented as contour plots in Figures 1a and 1b. Figure 1c shows the unsmoothed 18.2 μm image, which indicates the quality of the original data.

3. DISK MORPHOLOGY IN THE THERMAL INFRARED

The discovery images clearly showed the disk around HR 4796A to be extended at 18 μm, but both teams only marginally resolved it at 10 μm (J98; K98). Figure 1 demonstrates that the emission ridge corresponding to the edge-on disk is well resolved at both 10 and 18 μm in these new images. For comparison, the PSFs determined from nearby stars are presented in Figure 2 on both logarithmic and linear brightness scales. At 10 μm, the disk is evident as very low-level wings protruding from the strong stellar point source (which, for convenient display, is therefore plotted logarithmically in Fig. 1a). The ridge is much more prominent at 18 μm (plotted linearly in Fig. 1b). The line connecting the two outer peaks is oriented along P.A. = 26° ± 2°, and the maximum extent of the lowest 18 μm contour display in Figure 1 is about 3″.1, or 208 AU. The maximum extent at 10 μm is about 2″.8, or 85%–90% that of the 18 μm emission, and thus the 10 and 18 μm sources are roughly equal in size along the ridge. We also resolved the 18 μm disk along the minor axis, as indicated by the scans through the lobes and a comparison star shown in Figure 3.

Three peaks of comparable brightness are embedded in the 18 μm ridge. Each of the two outer 18 μm peaks, which
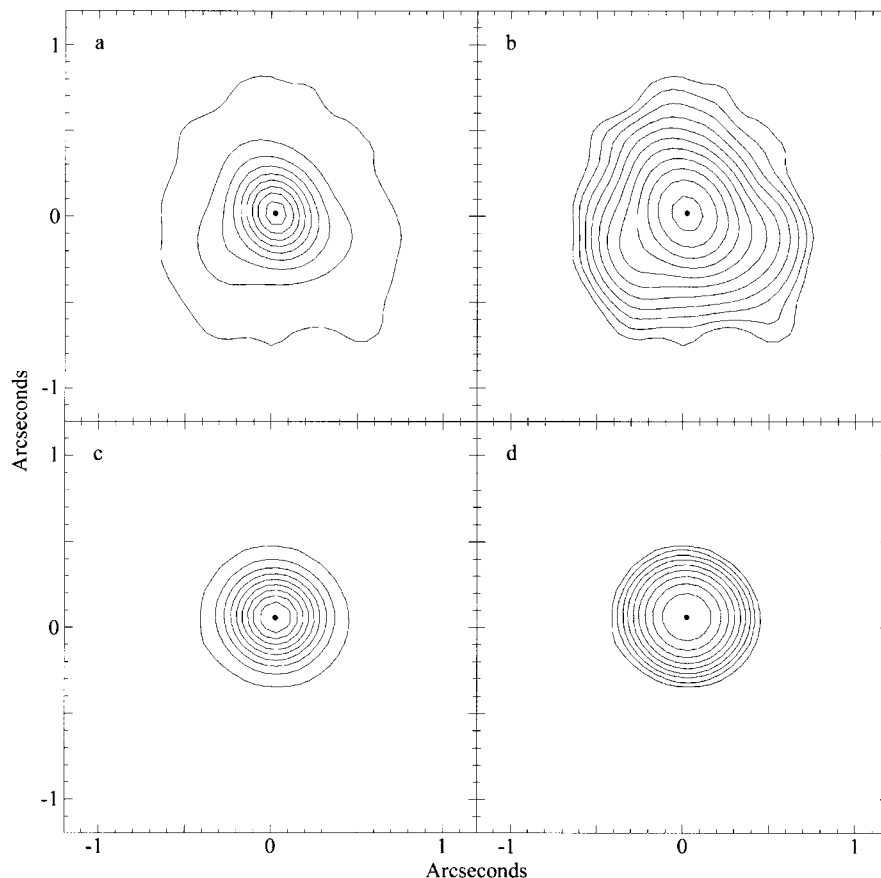

FIG. 2.—Plots of the point-spread functions (PSFs) at 10.8 and 18.2 μm based on observations of comparison stars. North is up, and east is to the left. All plots are normalized to a maximum value of 100 units located at the filled circle. (a) Linear 10.8 μm levels: 1, 12, 23, 34, 45, 56, 67, 78, and 89. (b) Logarithmic 10.8 μm levels: 1.3, 1.9, 2.8, 4.2, 6.2, 9.2, 13.7, 20.2, 29.9, 44.3, and 65.5. (c) Linear 18.2 μm levels: 8.0, 18.2, 28.4, 38.6, 48.8, 59.0, 69.2, 79.5, and 89.7. (d) Logarithmic 18.2 μm levels: 8.0, 10.6, 13.9, 18.4, 24.3, 32.1, 42.3, 55.9, and 73.7.
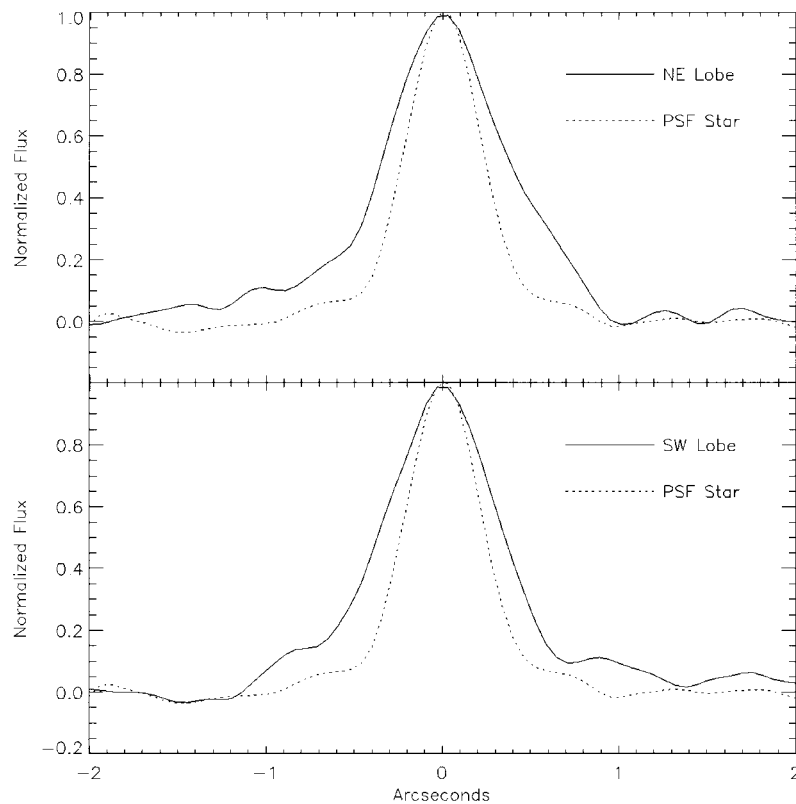
Fig. 3.—Comparison of minor-axis scans through the 18.2 μm lobes and a comparison star, which shows that the lobes are resolved along the minor axis of the disk. The northwest side of the scan is to the right (positive offsets).

we refer to as the lobes, is separated from the central peak by 0″.8 (54 AU). The brightest region within the central 18 μm contour is indicated in Figure 1b by a filled circle. That point is slightly offset from the centroid of the highest central contour; it lies on the line connecting the two lobes and halfway between them. By imaging sequentially at the two wavelengths with the Keck II visitor-port autoguider in operation, which facilitated accurate registration, we determined that the central 18 μm peak coincides with the 10 μm peak to within 0″.3. As described below, most of the 10 μm emission is direct starlight, and therefore the coincidence between the central 10 and 18 μm peaks implies that the central 18 μm peak also coincides with the star, which we therefore assume is coincident with the filled circle in Figure 1b. In the 10 μm contour plot in Figure 1a, we indicate (crosses) the location of the peaks of the 18 μm lobes. The 18 μm lobes clearly coincide with the 10 μm wings, and therefore much, possibly most, of the 10 μm–emitting dust must be mixed with, or identical to, the 18 μm–emitting dust. The 18 μm brightness at the lobes is comparable to that at the star, whereas their 10 μm brightness is only 4%–5% that at the star. The disk morphology that we see at 18 μm is consistent with that seen by K98 in their Keck images. K98 did not resolve the disk at 10 μm.

The mid-infrared radiation from HR 4796A originates both in the stellar photosphere and in dust that is heated by the starlight. The stellar photospheric flux densities at 10 and 18 μm are about 80% and 5%, respectively, of the total observed flux densities. Although the 18 μm stellar flux is a small fraction of the total, it contributes a large fraction of the emission of the central peak itself. To determine the contribution of the stellar photosphere to the image, we subtracted the stellar PSF from the image of HR 4796A

after registering the peaks and normalizing the comparison star's flux to that inferred for HR 4796A (Table 1). The PSF star was located near HR 4796A and observed just before and just after it. Due to the hexagonal shape of the Keck primary and secondary mirrors, the PSF is hexagonally shaped, so that, for the most accurate point-source subtraction or deconvolution, one cannot assume circular symmetry of the PSF. During the 18 μm observations of HR 4796A, the PSF rotated about 23° relative to the imager field of view (a rotation inherent in the altitude-azimuth mount). From the observed PSFs we constructed a time-averaged PSF appropriate to the rotational range of the PSF during our observations of HR 4796A.

The slightly smoothed (3 pixel) original and star-subtracted 18 μm images are shown in Figures 4a and 4b, respectively. The star was assumed to be coincident with the brightest part (Fig. 1b, filled circle), of the central maximum. Subtraction of the stellar flux removes the central peak, leaving a hole at that position. Because of the apparent absence in HR 4796 of significant dust hotter than about 110 K, Jura et al. (1995) concluded that the disk has a roughly 40 AU radius central hole in it. This conclusion was subsequently confirmed by the first direct images of the disk at ∼20 μm (J98; K98) and, more recently, by NICMOS images at 1–2 μm (Schneider et al. 1999; see below). We see the hole directly in our 18 μm image (Figs. 1b and 4a) as a depression between the central peak and each of the two lobes; it is obvious in the image with the starlight subtracted (Fig. 4b). Some tenuous emission may also be present in the inner region, i.e., the region within ∼0″.5 of the star. The appearance of this residual emission depends on how we characterize and position the subtracted stellar PSF. In the Appendix we address briefly some aspects of
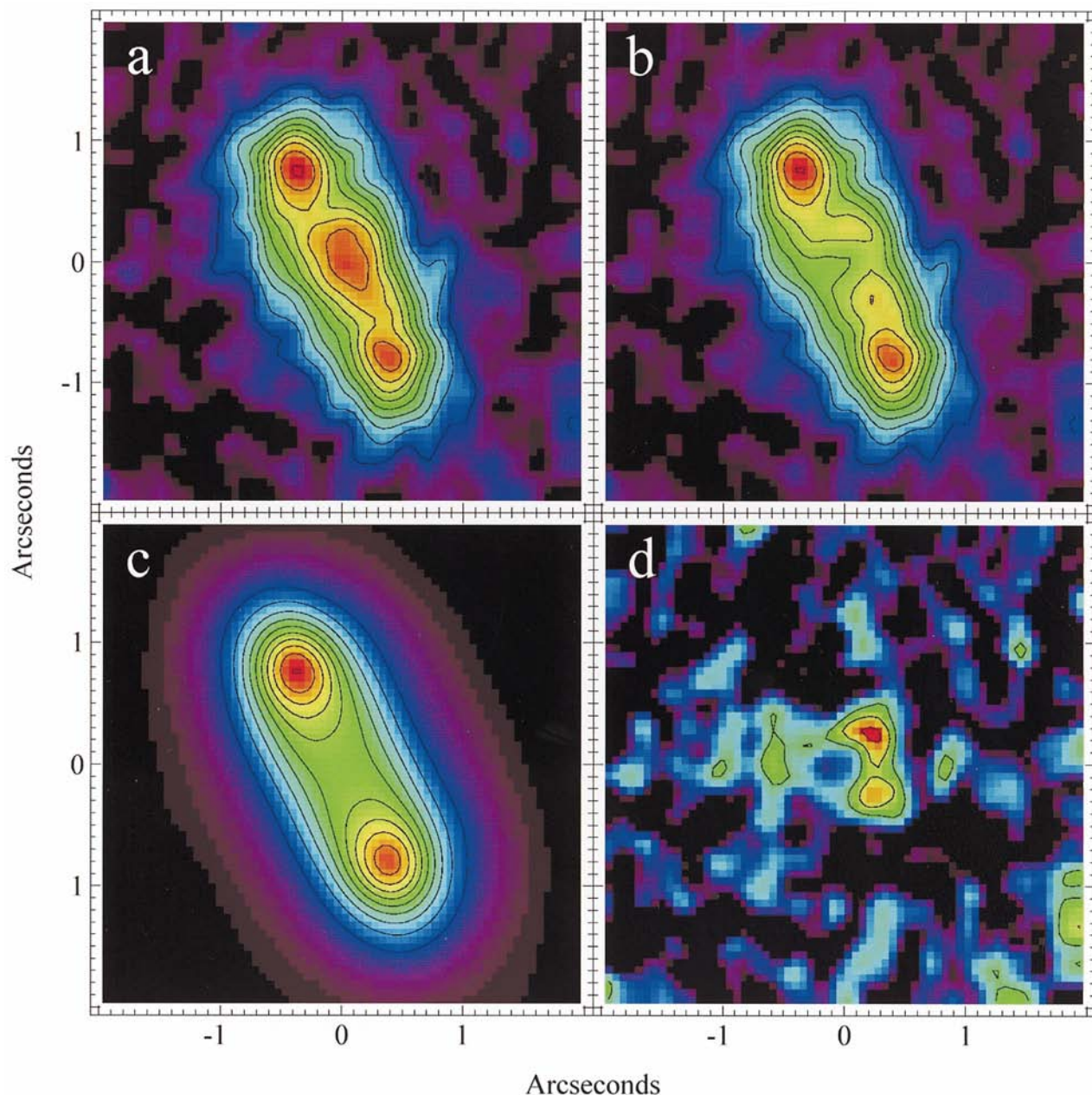
FIG. 4.—Comparison of the 18.2 μm images of HR 4796A with the model brightness distribution. North is up, and east is to the left. Overlaid contour levels (mJy arcsec^{-2}) are linearly spaced. (a) Observed image smoothed with 3 pixel Gaussian, with contour levels the same as in Fig. 1b. (b) Observed image after subtraction of stellar photospheric emission. Contour levels: 58, 93, 128, 163, 198, 234, 269, 304, 339, and 374. (c) Model brightness distribution. (d) Residual emission, corresponding to the difference between the star-subtracted and model brightness distributions. Contour levels: 20, 40, and 60.

how the computed residual is affected by slight errors in the position and width of the PSF used to subtract HR 4796A's starlight.

We also subtracted the stellar photospheric 10 μm flux from the 10 μm image. The central hole is evident in that subtracted image, but the disk is so much fainter than the star that the subtraction procedure is very uncertain. Therefore, we do not have confidence in the accuracy of this result, insofar as it bears on the structure of the inner part of the emitting region. However, those 10 μm results are useful in the context of estimating the characteristic size of the mid-infrared–emitting particles (§ 6).

There is some evidence that the lobes are not of equal maximum brightness: the northeast lobe is 5.9% $\pm$ 3.2% brighter than the southwest lobe, where this asymmetry

corresponds to the difference in the lobe peak brightnesses divided by their mean. This value for the asymmetry includes a 0.8% correction for an asymmetry in the PSF. The formal statistical significance of the brightness asymmetry of the lobes is therefore 1.8σ. The brightness asymmetry itself was determined by fitting a polynomial to a 10 pixel $\times$ 10 pixel (0″.6 $\times$ 0″.6) region approximately centered on each peak. The uncertainty associated with this asymmetry was established by convolving the best-fit model (§ 4) with a Gaussian approximation to the PSF, applying Gaussian noise like that observed across the array, and fitting the polynomial as mentioned above. After repeating this procedure 50,000 times, we computed the rms deviation, which constituted the formal uncertainty. This asymmetry may also be apparent in the 10 μm image

(particularly in the scan in Fig. 8b, discussed below) and in the NICMOS image (Schneider et al. 1999). The asymmetry is discussed in a much broader context in the companion paper by W99. We briefly comment on it below.

4. MODELING THE BRIGHTNESS DISTRIBUTION

J98 and K98 modeled their ~ 20 μm images of HR 4796A to infer structural properties of the disk. Both models assumed optically thin, passive disks in which the dust particles have an infrared emission efficiency varying with wavelength as λ^{-1}. J98 found that an edge-on dusty disk with an inner hole radius somewhere in the range 40–80 AU provides an adequate fit to the spectral energy distribution and the image. The higher resolution Keck image obtained by K98 more tightly constrains their thin-disk model, from which they infer an inner hole radius of 55 ± 15 AU and a disk inclination of $18°$ ($+9°$, $-6°$) from edge-on.

In the companion paper, W99 present results of modeling the 18 μm brightness distribution of HR 4796A. Since it is relevant to our estimate of the grain size and to the comparison of our results to the HST/NICMOS observations, we summarize the model here. W99 consider the dynamical interaction of a circumstellar disk and a stellar or planetary companion, a study initially motivated by the desire to understand how such interactions generate asymmetries and other structures in circumstellar disks. A distribution of orbiting dust particles is gravitationally perturbed by a companion, and W99 examine the resultant orbital and density distributions for dust grains of a given size and composition. W99 ignore the effects of radiation pressure, assuming, in effect, that large, dynamically stable dust grains, with $\beta \approx 0$, orbit HR 4796A; β is the ratio of the radiation pressure force to the gravitational force on a particle (called δ, the overpressure ratio, by Backman & Paresce 1993). However, at least in the context of Mie theory, we know that these large particles are not the ones that we observe in the mid-infrared. As discussed in § 6, the mid-infrared–emitting particles, if they are Mie spheres of astronomical silicates (Draine & Lee 1984), are ~ 2–3 μm in diameter, with the corresponding value $\beta \approx 2$. Radiation pressure will drive particles with such a high value of β out of the system on hyperbolic orbits in a few hundred years. Based on this negligible lifetime and on estimates of the particle number density and collision rates in the disk, W99 (see § 6 below) conclude that these grains must be collision fragments of much larger particles. The spatial distribution of larger particles in the HR 4796A disk is unknown, so, as an alternative, W99 assume that larger particles are distributed essentially like the smaller, 2–3 μm size, Mie grains emitting the observed mid-infrared radiation. By accounting for the temperature dependence of the dust as a function of distance from the star, they determine the spatial distribution of the mid-infrared–emitting grains from our 18 μm image.

The model disk is not flat but flared, with a distribution of orbital proper inclinations and proper eccentricities identical to those of the main-belt asteroids in our own solar system. The distribution of semimajor axes for the particles is assumed to follow the relation $n(a) \propto a^\gamma$, where $n(a)$ is the number of orbits per unit semimajor axis. For particle orbits that are circular, which is approximately the case for the model orbits, the surface number density as a function of distance r from the star is therefore proportional to $r^{\gamma-1}$. The largest value, a_{max}, used for the semimajor axis of the

dust orbits is 130 AU, although the results of the modeling are not sensitive to this value, since relatively little flux arises near the outer edge of the disk. Key model parameters that are varied to match the observations are (1) the exponent γ; (2) the minimum value, a_{min}, of the dust semimajor axis, which controls the diameter of the central clearing; (3) the normalization of the density distribution; and (4) the inclination of the disk symmetry plane to the line of sight. In addition, observed asymmetries in the brightness distribution are modeled by adjusting the common forced eccentricity and the direction of the forced pericenter of the disk particle orbits.

Figure 4c shows the model brightness distribution at 18 μm that is the best fit to the star-subtracted image in Figure 4b. The residual (observed minus model) is shown in Figure 4d. The model fits the lobes well, with nearly all of the residual flux located within $0\rlap{.}''4$ of the star. We are not certain of the nature of the residual flux. Some of it may represent real flux from HR 4796A's inner disk, but some of it may result from imperfect subtraction of the stellar photospheric flux stemming from variations in the seeing not manifested in the PSF-star images (which were of shorter duration). We briefly address this issue in the Appendix.

The model disk inclination is $13° \pm 1°$ from edge-on. A flat disk would be modeled as more face-on than this, since the disk flaring that we assume in the model accounts for some of the resolved disk extension that we see along the minor axis (Fig. 3). For the distribution of semimajor axes, $\gamma = -2 \pm 1$. The resultant model distribution of surface number density (i.e., integrated normal to the disk) of 2.5 μm grains is shown in Figure 5 in the form of a radial cut through the azimuthally averaged disk (solid curve). The surface density is relatively sharply peaked near 70 AU. Exterior to this position, the surface density decreases with distance approximately as r^{-3}. Interior to this position, the surface density drops steeply by a factor of 2 between 70 and 60 AU, falling to zero by 45 AU. The model fit implies $a_{min} = 62 \pm 2$ AU, but because the dust particle orbits are assumed to be noncircular, the hole is not sharply defined in the models; i.e., the orbital eccentricity results in a small range in a particle's radial location, which softens the hole's edge. Flat-disk models based on the disk-discovery images indicate comparable values for the hole radius (J98; K98), but the dynamical models considered here provide an a priori basis for understanding why a hole should have an indistinct, or soft, edge.

How empty is the hole in the disk? We can estimate the optical depth in the hole by comparing the brightness of the residual emission there (assumed to represent an upper limit to emission from dust) to the observed brightness of the lobes. Consider first the optical depth in the disk lobes. The southwest lobe is 54 AU in projection from the star. The model temperature there is 113 K (compared to the blackbody temperature of 81 K) and, ignoring projection effects, the corresponding edge-on optical depth at 18 μm is ~ 0.002. The residual emission (observed minus model; Fig. 4d) at 20 AU ($0\rlap{.}''3$ from the star) is typically 0.2 times that of the lobes. The model temperature at 20 AU is 163 K, and thus the 18 μm edge-on optical depth there is $\sim 5 \times 10^{-5}$, which is about 3% of that of the lobes. Assuming that the ratio of the face-on optical depth to the edge-on optical depth in the hole is comparable to that ratio at the lobes, then the average optical depth of 18 μm–emitting dust in
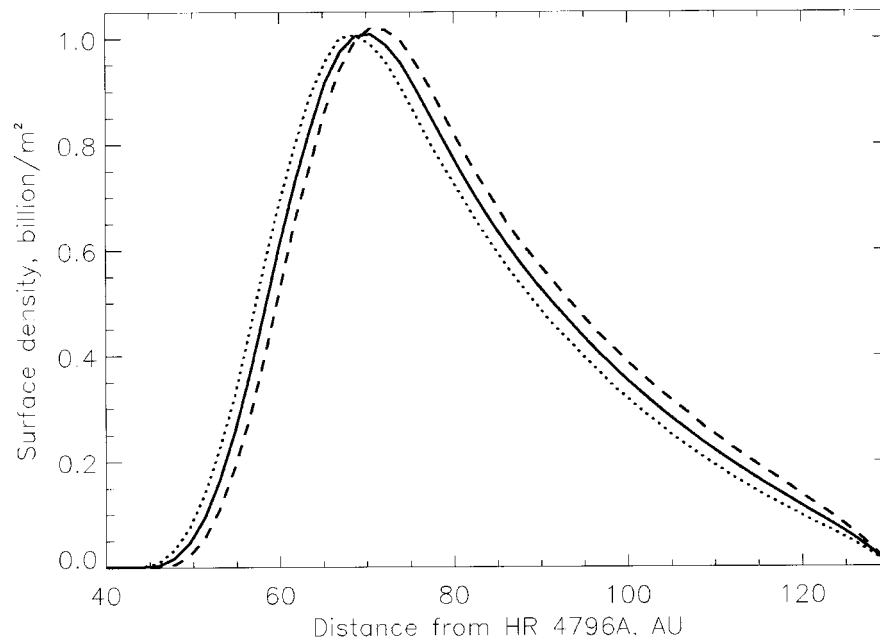
FIG. 5.—Plots of the surface number density of the 2.5 μm dust grains in the disk derived from modeling the 18 μm brightness distribution. The solid curve is the azimuthal average of the surface number density, the dotted line and the dashed line indicate the density through the disk in the direction of and away from, respectively, the stellar companion's pericenter. The relative displacement of the dotted and dashed lines indicates the scale of the displacement of the disk center from the star.

the hole appears to be about 3% of that in the main part of the disk at 60–100 AU from the star. If any of the residual emission results from poor PSF subtraction and is not intrinsic to the source, the optical depth of the dust in the hole could be even less than this. The central cleared region appears to be relatively very empty.

There has been speculation about the causes of holes in the centers of circumstellar disks (Lagage & Pantin 1994; Jura et al. 1998; Strom, Edwards, & Skrutskie 1993; Roques et al. 1994; J98; K98), and the disk in HR 4796A is likely to become a strong focus for these discussions (e.g., Jura et al. 1995; W99). We only wish to emphasize here that the possible disk brightness asymmetry is an interesting and perhaps unexpected manifestation of the central hole. The brightness asymmetry in the model results from the gravitational perturbation of the disk particle orbits by the low-mass companion HR 4796B even if the companion's orbit is only moderately eccentric (W99). To first order, the effect of the perturbation is to shift the center of symmetry of the circular disk from HR 4796A toward the companion's apocenter, where the companion spends most of its time; i.e., the long-term average of the perturbation on the disk particles is directed toward the companion's apocenter. The side of the disk, and therefore the hole edge, that is closest to the companion's pericenter is shifted closer to the primary star and is therefore warmer ("pericenter glow"). The pericenter glow is a direct result of there being a hole in the disk. If this model is valid and these perturbations do arise from HR 4796B, then HR 4796B's pericenter must be located northeast of HR 4796A, and HR 4796B is currently located near its apocenter southwest of HR 4796A. The scale of the shift of the disk's center of symmetry is indicated by comparing the dashed and dotted curves in Figure 5, which shows the density distribution through the disk toward and away from the stellar companion's pericenter. The disk is shifted only a few AU, which, while a small amount, leads to

an arguably measurable brightness asymmetry. The perturber responsible for the shift of the disk need not be exterior to the disk. A star or planet within the hole could cause the same effect (W99); however, based on near-infrared speckle observations (Jura et al. 1995), the mass of any stellar companion located between 11 and 120 AU from HR 4796A must be less than 0.13 $M_\odot$. The fact that we may be detecting a brightness asymmetry resulting from a shift of a few AU in the disk centroid implies that the detection of significant dynamical effects on circumstellar disks by stellar or planetary companions is now within reach. The *HST*/NICMOS images presented by Schneider et al. (1999) may confirm this pericenter glow (§ 5 below).

5. COMPARISON OF MID-INFRARED AND *HST*/NICMOS IMAGES

Schneider et al. (1999) have imaged the HR 4796A disk at 1.1 and 1.6 μm with NICMOS. They used a 0″6 diameter coronagraphic spot, but, owing to a variety of instrumental effects, the data in a $\sim$1″3 diameter region are unusable. Their images show clearly what appears to be a relatively narrow ring inclined to the line of sight. Assuming that the ring is intrinsically circular, they determine a major-axis position angle of 26°.8 $\pm$ 0°.6 and an inclination of the line of sight of 73°.1 $\pm$ 1°.2, in agreement with our estimates (W99; see §§ 3 and 4 of this paper) and those of K98. The mean radius of the ring is 70 AU, and, after quadratic subtraction of the PSF, the full width of the annulus is estimated to be 17 AU (Schneider et al. 1999). The relatively sharp maximum in the density near 70 AU determined from our modeling of the OSCIR observations agrees precisely with the value derived by Schneider et al. (1999) for the mean radius of the ring based on the NICMOS observations. We now consider a more detailed comparison.

In Figure 6 we show our 10 and 18 μm contours overlaid on the 1.1 μm NICMOS image. Keeping in mind the differ-
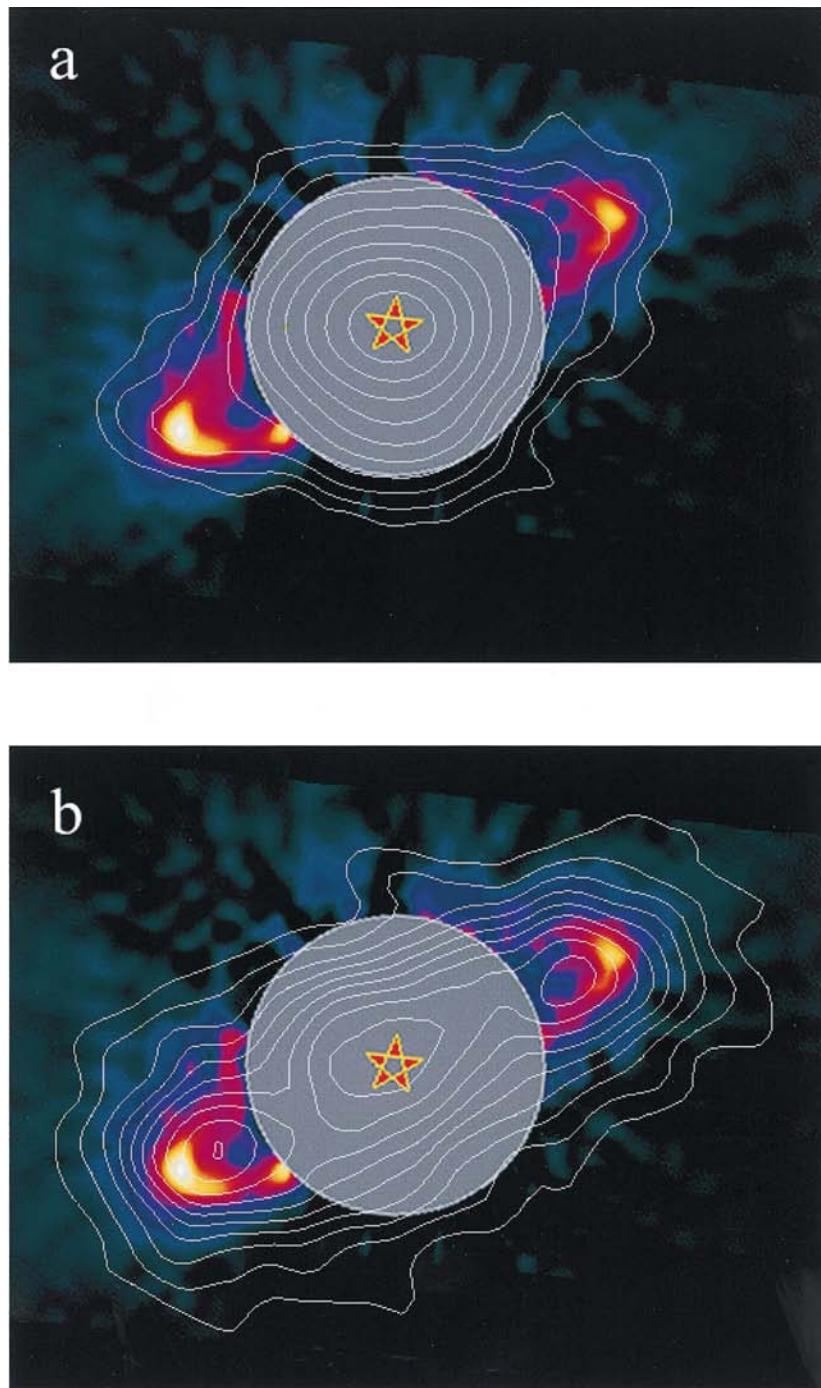
Fig. 6.—Overlay of (a) 10.8 and (b) 18.2 μm contours on the 1.1 μm *HST*/NICMOS image of HR 4796A disk from Schneider et al. (1999). The angular resolutions (FWHM) of the images are: 0″.12 at 1.1 μm; 0″.32 at 10.8 μm; 0″.45 at 18.2 μm. In both images, east is approximately down, and north is to the left (see Schneider et al. 1999). In this orientation, the companion star HR 4796B is located to the upper right.

ences in the resolutions of the images (FWHM: 0″.12 at 1.1 μm; 0″.32 and 10.8 μm; 0″.45 at 18.2 μm), we see that the overall coincidence of the mid-infrared and near-infrared emission is excellent. However, the 18 μm lobes are located noticeably closer to the star than are the bright 1.1 μm peaks. The peaks of the 18 μm lobes are separated by 1″.73, compared to 2″.10 for the peak-intensity positions at 1.1 μm (Schneider et al. 1999). To assess the nature of this offset, we considered a perfectly thin ring (annulus) of dust with uniform number density and the temperature distribution derived in the W99 models. We assumed a mean annular

radius of 70 AU and an annular width of 17 AU and computed the 18.2 μm brightness at each point in the ring, which we convolved with the observed 18.2 μm PSF. In Figure 7 we compare the brightness distribution along the major axis expected for this convolved model to the observed brightness distribution.

This comparison implies that ∼60% of the 0″.37 difference in the separation of the peaks at 1.1 and 18.2 μm results from the lower resolution of the 18 μm image. Figure 7 indicates that the uniform-annulus model results in an 18 μm distribution with lobes displaced to larger radii and
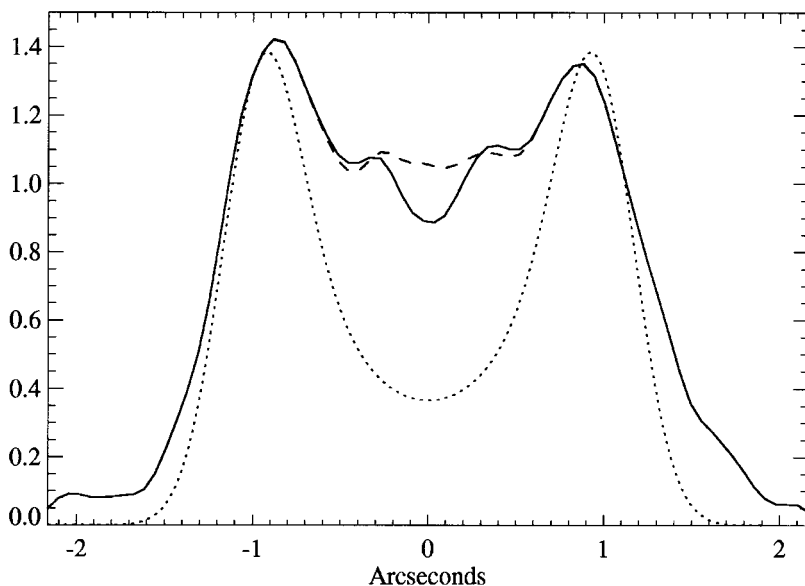
FIG. 7.—Comparison of major-axis cut through the lobes of our 18 μm star-subtracted image (*solid curve*) to that expected (*dotted curve*) from the simplest disk model inferred by Schneider et al. (1999) from their NICMOS image. The left side of the scan is northeast of the star. The model disk is a thin annulus with a mean radius of 70 AU, a width of 17 AU, a uniform density, and the temperature falloff with radius determined by W99. The Schneider et al. (1999) model has been convolved with the observed 18 μm PSF. The dashed curve shows the result of subtracting from the observations a stellar PSF that has an additional 0″.35 seeing, as discussed in the Appendix.

appearing somewhat narrower than actually observed. The discrepancy in slope is primarily on the insides of the lobes. The observed outer slope of the northeast lobe is well matched by the model, while the match of the southwest lobe is noticeably poorer. We do not think that these differences between the NICMOS-based model and the 18 μm observations result from inaccurate subtraction of the stellar PSF from the 18 μm image. Figure 7 gives some indication of the small dependence of the shape inferred of the inside of the disk lobes on the assumed shape of the PSF; we show the flux distributions resulting from use of the nominal, observed PSF (*solid curve*) and the same PSF with an additional 0″.35 of seeing (*dashed line*; see Appendix). Rather, the difference in the observations and the brightness expected from the model may result from the annulus having a somewhat soft inner edge. Primarily because of the lower resolution of the 18 μm observations, a more gradual density falloff on the inside of the annulus will both shift the observed peaks inward and decrease the inner slope of the lobes. The excellent agreement in the location of the peak density in the disk, as determined from models of the OSCIR images, and the average radius of the annulus determined from models of the *HST*/NICMOS images, suggests that it is this inner density rolloff, or a similar refinement such as excess emission in the hole, that accounts for the relative locations of the observed emission peaks in the two data sets. A slower density falloff on the outside of the annulus would elevate the 18 μm wings, although we see this only on the southwest side of the disk. As shown by W99 and discussed in the previous section, one may account for a soft-density falloff on the inside of the annulus by the kinds of dynamical properties anticipated (and assumed in the W99 models) for the orbiting dust particles.

Figure 6 shows that at 1.1 μm the northeast side of the annulus is noticeably brighter than the southwest side. This asymmetry is not evident in the 1.6 μm NICMOS image.

This asymmetry may support our, albeit marginal, detection of the pericenter glow at 18 μm. However, one is seeing emission from dust particles at 18 μm but scattering from dust (and probably a different population) at 1–2 μm. We speculate that the mass shift that may result in the enhanced lobe brightness at 18 μm could also enhance the scattering of light there. Detailed models that incorporate realistic scattering functions must be carried out to explore this interesting possibility.

6. THE MID-INFRARED–EMITTING DUST

6.1. The Characteristic Particle Size

Circumstellar dust spans a range of compositions and sizes. However, for a given composition, one can derive from observations at two wavelengths a unique particle size that is arguably characteristic of the dust responsible for that emission. The basis for this estimate is that the emission efficiency, and therefore the temperature, of a dust particle depends on its size. We made an initial estimate of the size of dust particles in HR 4796A by taking the ratio of the 10 and 18 μm fluxes in the lobes (after correcting for the different PSFs at the two different wavelengths) and comparing it with that expected from Mie silicate spheres of different sizes, which have different emission efficiencies and consequently different temperatures. The formal value of this initially estimated diameter was 2.5 μm. (Mie silicate grains of this diameter have infrared emission efficiencies varying approximately as $\lambda^{-1.9}$.) This initial estimate was then used to do the modeling described in § 4, which was repeated using 2 and 3 μm diameter particles. In Figure 8a we show the resultant scan along the major axis of the 18 μm image from which the stellar photospheric emission (using the nominal PSF; see Appendix) has been subtracted. The model discussed above provides a good fit to the 18 μm lobe structure for a range of assumed dust sizes. However, Figure 8b shows how the 10 μm brightness constrains the
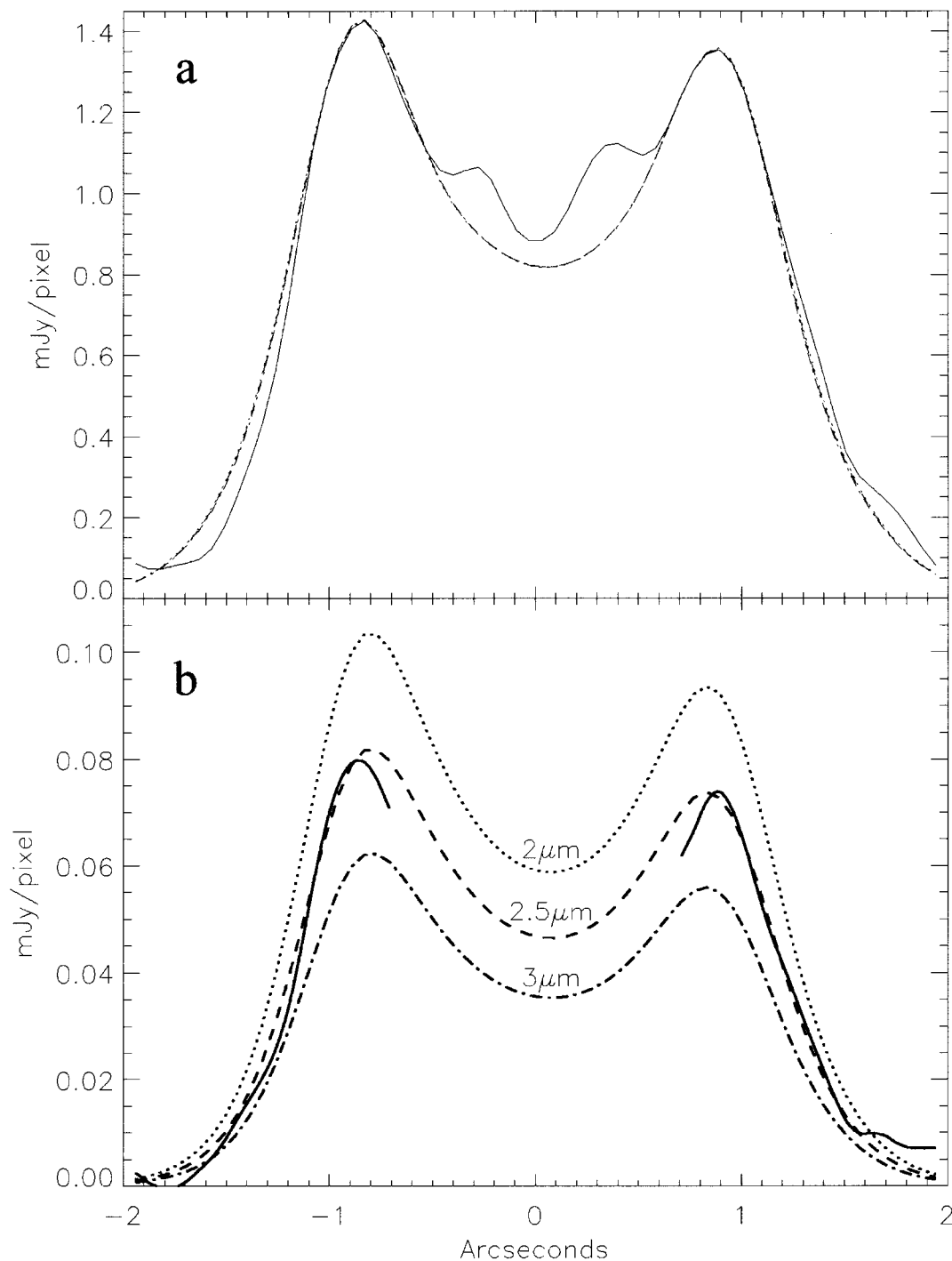
FIG. 8.—Comparison of (a) the star-subtracted 18.2 μm and (b) 10.8 μm scans, indicated as solid lines, along the disk major axis of the HR 4796A disk. The left side of each scan is northeast of the star. In the 18 μm scan, the features within ~0.″3 of the stellar position are probably artifacts resulting from imperfect PSF subtraction. Only the lobes of the 10 μm scan are shown (see text). The 18 μm brightness distribution has been modeled, as described in the text, using spherical Mie silicate particles that are 2, 2.5, and 3 μm in diameter. The corresponding scan of the 10.8 μm flux distribution expected from a disk composed of each of these particles indicates that the 10.8 μm brightness in the lobes is best fitted by 2.5 μm diameter particles. Thus, in the context of Mie theory, the grains are constrained to be a few microns in diameter.

diameter to 2.5 μm, consistent with our original estimate. We conclude that, under the assumption that the particles we see in the lobes are astronomical silicate Mie spheres, 2–3 μm diameter grains provide a reasonable fit to the lobe mid-infrared colors. Of course, based on studies of interplanetary dust particles in our solar system (e.g., Gustafson 1994), it is evident that the dust particles in HR 4796A's disk

are unlikely to be simple spheres, the implications of which we are in the process of considering.

6.2. Particle Evolution

We can consider the effects of the stellar radiation on 2.5 μm size grains by estimating the value of the parameter β, the ratio of the radiation pressure force to the gravitational

force on a particle. As summarized in Artymowicz (1988) and elsewhere, $\beta \propto \langle Q_{pr} \rangle (L_*/M_*)/R\rho$, where R is the particle radius, ρ is its density, $\langle Q_{pr} \rangle$ is the radiation pressure efficiency averaged across the stellar spectral energy distribution, and L_*/M_* is the ratio of the stellar luminosity and mass. W99 have computed the value of β for 2.5 μm diameter silicate spheres near HR 4796A; they assumed $L_* = 21\ L_\odot$, $M_* = 2.5\ M_\odot$, and $\rho = 2.5$ g cm^{-3}, and they compute $\langle Q_{pr} \rangle$ using a stellar spectral energy distribution for the A0 V star Vega (M. Cohen 1999, private communication). They derive the value $\beta = 1.7$ for the grains that characterize the mid-infrared–emitting particles in HR 4796A's disk. If one takes into account the differences in spectral type and assumed grain density, this value agrees reasonably well with the one that can be derived from the results in Artymowicz (1988; see his Fig. 1), who computed β for the star β Pic and for a variety of grain materials including the astronomical silicates of Draine & Lee (1984). Dust grains that are created in collisions, and for which β is greater than ~ 0.5, have hyperbolic orbits; they are blown beyond ~ 100 AU and out of the system on essentially free-fall timescales, on the order of a few hundred years. Thus, the 2–3 μm grains we see orbiting HR 4796A are not primordial; one expects very few of them in this disk (see also Jura et al. 1995). The detailed analysis by W99 (see also Artymowicz 1997) implies that the collisional lifetime of the dust in HR 4796A is roughly 10^4 yr across the disk. The mid-infrared–emitting particles are probably relatively recent fragments of collisions that dominate both the creation and destruction of dust there.

7. SUMMARY AND CONCLUSIONS

1. Our new 10 and 18 μm images of the circumstellar disk around the A0 Vega-type star HR 4796A images show extended, well-resolved emission at 10 μm in addition to the previously discovered 18 μm emission (J98; K98). The resolution of both images is close to the Keck diffraction limit. The size of the 10.8 μm–emitting region is comparable to that at 18 μm, implying that most of the 10 μm–emitting particles are mixed with, or identical to, those emitting at 18 μm.

2. Modeling of the disk brightness distribution (W99) implies that a pronounced maximum in the surface density occurs at approximately 70 AU from the star. This value equals the mean annular radius deduced by Schneider et al. (1999) from their *HST*/NICMOS images. The best-fit model surface density exterior to 70 AU falls steeply with distance as r^{-3}. Interior to 70 AU, the density drops steeply by a factor of 2 between 70 and 60 AU, falling to zero by 45 AU, which corresponds to the edge of the previously discovered central hole; in the context of the dynamical models, this "soft" edge for the central hole results from the fact that the dust particle orbits are noncircular.

3. Based on the images, the optical depth in the central clearing zone, or hole, is $\sim 3\%$, or less, of that in the main part of the disk. Thus, the hole is indeed relatively empty.

4. We present tentative evidence (1.8σ) that the 18 μm lobes are of unequal brightness. Detailed modeling of the 18 μm brightness distribution based on dynamical considerations and presented in a companion paper (W99) indicates that such a brightness asymmetry could result from gravitational perturbation of the disk particle orbits by the low-mass stellar companion or a planet. The perturbation shifts the disk center of symmetry away from the companion's pericenter; to first order, this shift corresponds to a spatial shift of the center of the circularly symmetric disk. This shift brings the inside edge of the annulus closer to HR 4796A, which makes that edge warmer and more infrared-emitting ("pericenter glow") than the other side of the annulus. This measurable brightness asymmetry corresponds to a spatial shift of the disk of only a few AU, and so the detection of even fairly complex dynamical effects of planets on disks appears to be within reach. The recent 1.1 μm NICMOS image (Schneider et al. 1999) may show evidence in support of the pericenter glow.

5. We compare our 10 and 18 μm images with recent NICMOS images of HR 4796A at 1.1 and 1.6 μm that show what appears to be a relatively narrow ring, or annulus, inclined to the line of sight and with a mean radius of 70 AU and an annular width of ~ 17 AU. The overall coincidence of the near-infrared and mid-infrared structure is excellent. However, even after accounting for differences in angular resolution, we find that the 18 μm distribution expected from the NICMOS-based model differs somewhat from the observed distribution. These differences suggest that the annulus has a "soft" inner edge, which may correspond to the density falloff expected from considerations of particle dynamics.

6. Using the 10 and 18 μm images, we estimate that the mid-infrared–emitting dust particles in the main part of the disk have a characteristic diameter of ~ 2–3 μm. This estimate is based on the assumption that the particles are Mie spheres composed of astronomical silicates. The corresponding value of the parameter β, the ratio of the radiation-pressure force to gravitational force on the particle, is 1.7. Particles with $\beta > 0.5$ are expected to be quickly blown out of the system. We conclude that the mid-infrared–emitting particles in the HR 4796A disk are not primordial, but rather that they are relatively recent and transient collision fragments.

APPENDIX

We pointed out in § 3 that some of the inner tenuous emission (within 0″.5 of the star) apparent in the star-subtracted 18 μm image of HR 4796A (Fig. 4*b*) and as residual emission in Figure 4*d* may be an artifact resulting from the use of an unsuitable

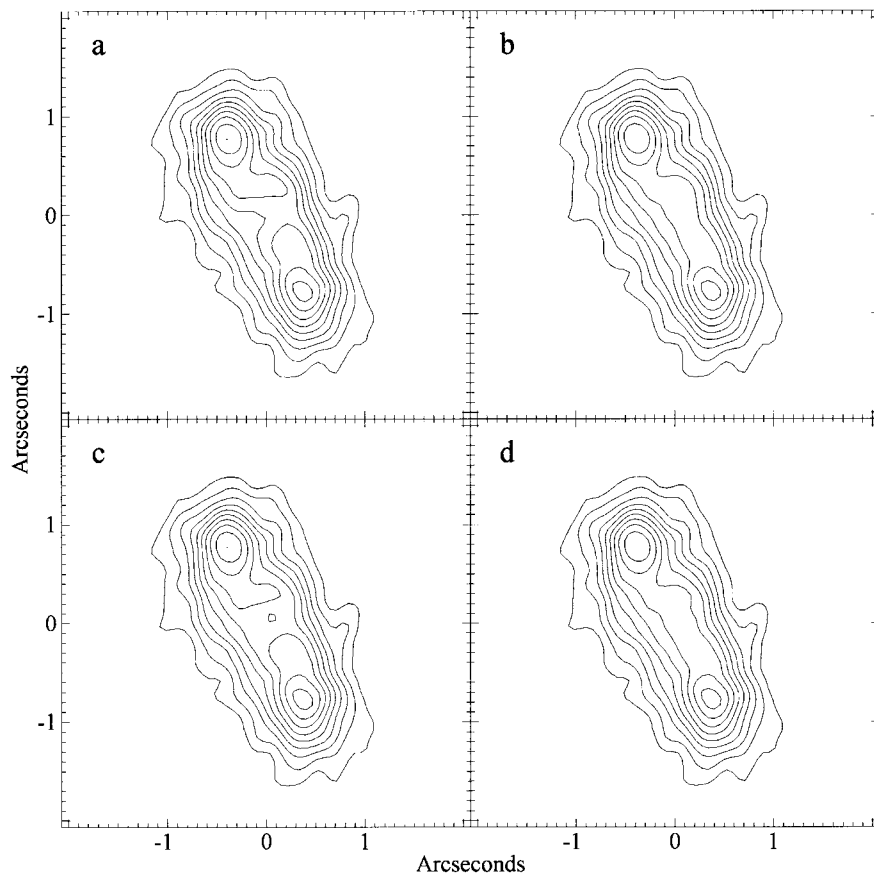Fig. 9.—Comparison of the 18 μm disk emission resulting from the subtraction from the observed image (Fig. 1b) of a modest range of stellar point-spread functions normalized to the expected flux of the star HR 4796A. North is up, and east is to the left. As discussed in the Appendix, the intent of this exercise is to illustrate the effect on the inferred inner disk structure of the use of an inaccurate, or slightly mispositioned, PSF. (a) Nominal observed PSF (FWHM =0″.45) subtracted at brightest spot (Fig. 1b, filled circle). (b) Seeing-convolved PSF (seeing FWHM =0″.35) subtracted at brightest spot. (c) Nominal observed PSF subtracted at centroid of highest central contour. (d) Seeing-convolved PSF subtracted at centroid of highest central contour.

PSF. This mismatch could occur if there are low-frequency seeing components sampled during the ~1 hr of chopped integration time on HR 4796A (Table 1) that are not sampled during the much shorter (~1 minute) integration time on the nearby star used to determine the PSF. (Given the limited amount of available observing time, it is unrealistic to observe the PSF star for the same amount of time that we observe the program objects.) Here we briefly examine this issue.

Figure 9a presents the star-subtracted 18 μm image presented previously in § 3 (Fig. 4b). That image resulted from the subtraction of HR 4796A's direct starlight (photospheric emission) using the observed stellar PSF (referred to as the nominal PSF) and assuming that the stellar peak is coincident with the location of maximum 18 μm brightness (Fig. 1, filled circle). Figure 9b shows the result of instead subtracting a somewhat broader PSF obtained by convolving the nominal PSF with a Gaussian profile with a FWHM of 0″.35. This might represent some additional seeing that could have affected the image of HR 4796A but not the observed PSF star image. In Figures 9c and 9d, we repeat this exercise, but with the star assumed to be at the centroid of the highest central contour indicated in Figure 1b, i.e., at 0″.1 west-northwest of the filled circle in Figure 1b. The intent of this exercise is to illustrate the sensitivity of the residual inner structure to the assumed stellar location.

We see that even this modest amount of extra "seeing" results in a star-subtracted image of HR 4796A that is noticeably less structured at the disk center. This comparison is also shown in the scans in Figure 7. Likewise, slight errors in positioning the star result in some differences in the inferred inner-disk structure. However, although the emission structure differs somewhat, the integrated residual flux is virtually unchanged, since the stellar flux is the same in both cases. As we have noted, the light cirrus evident throughout much of our Keck run may have resulted in poor photometric conditions, but we do not think this is the source of the residuals: the photometry is generally consistent to within ~20%, and even an error this large in the PSF flux normalization would only marginally effect the residual.

We conclude that the detailed structure of the inner disk (within 0″.5 of the star), as inferred from the star-subtracted image or the resultant image of the residual emission (e.g., Fig. 4d), must be viewed with caution. However, the integrated residual flux is more robust and may be real. If so, it may correspond to low-level dust emission from within the central clearing.

REFERENCES

Artymowicz, P. 1988, ApJ, 335, L79
———. 1997, Annu. Rev. Earth Planet Sci., 25, 175
Backman, D., & Paresce, F. 1993, in Protostars and Planets III, ed. E. Levy
    & J. Lunine (Tucson: Univ. Arizona Press), 1253
Beckwith, S. V. W., & Sargent, A. I. 1993, in Protostars and Planets III, ed.
    E. Levy & J. Lunine (Tucson: Univ. Arizona Press), 521
Draine, B. T., & Lee, H. M. 1984, ApJ, 285, 89
Greaves, J. S., et al. 1998, ApJ, 506, L133

Grün, E., et al. 1985, Icarus, 62, 244
Gustafson, B. Å. S. 1994, Annu. Rev. Earth Planet. Sci., 22, 553
Holland, W. S., et al. 1998, Nature, 392, 788
Jayawardhana, R., Fisher, S., Hartmann, L., Telesco, C., Piña, R., & Fazio, G. 1998, ApJ, 503, L79 (J98)
Jura, M. 1991, ApJ, 383, L79
Jura, M., Ghez, A. M., White, R. J., McCarthy, D. W., Smith, R. C., & Martin, P. G. 1995, ApJ, 445, 451
Jura, M., Malkan, M., White, R., Telesco, C., Piña, R., & Fisher, R. 1998, ApJ, 505, 897
Jura, M., Zuckerman, B., Becklin, E. E., & Smith, R. C. 1993, ApJ, 418, L37
Kalas, P., & Jewitt, D. 1995, AJ, 110, 794
———. 1997, Nature, 386, 52
Koerner, D. W., Ressler, M. E., Werner, M. W., & Backman, D. E. 1998, ApJ, 503, L83 (K98)

Kurucz, R. L. 1979, ApJS, 40, 1
Lagage, R., & Pantin, E. 1994, Nature, 369, 628
Lissauer, J. J. 1993, ARA&A, 31, 129
Podosek, F. A., & Cassen, P. 1994, Meteoritics, 29, 6
Roques, F., Scholl, H., Sicardy, B., & Smith, B. A. 1994, Icarus, 108, 37
Schneider et al. 1999, ApJ, 513, L127
Smith, B. A., & Terrile, R. J. 1984, Science, 226, 1421
Stauffer, J. R., Hartmann, L. W., & Navascues, D. B. 1995, ApJ, 454, 910
Strom, S. E., Edwards, S., & Skrutskie, M. F. 1993, in Protostars and Planets III, ed. E. Levy & J. Lunine (Tucson: Univ. Arizona Press), 837
Telesco, C. M., Becklin, E. E., Wolstencroft, R. D., & Decher, R. 1988, Nature, 335, 51
Wyatt, M. C., Dermott, S. F., Telesco, C. M., Fisher, R. S., Grogan, K., Holmes, E., & Piña, R. K. 1999, ApJ, 527, 918 (W99)